Proceedings of the 28th IEEE
EMBS Annual International Conference
New York City, USA, Aug 30-Sept 3, 2006

Noise Analysis for Multi-slice Radio Frequency Current Density Imaging

Dinghui Wang, Tim P. DeMonte, *Member, IEEE*, Michael L. Joy, *Member, IEEE*, and Adrian I. Nachman

Abstract— **Radio frequency current density imaging (RF-CDI) is an imaging technique that measures current density distribution at the Larmor frequency utilizing magnetic resonance imaging (MRI). The multi-slice RF-CDI sequence has extended the ability of RF-CDI to image multiple slices and thus has enhanced its capacity for biomedical applications. In this paper, the influence of MRI random noise on the sensitivity of multi-slice RF-CDI measurement is studied. The formula of current noise is derived, which is verified by both simulation and phantom experiments. A 3-D finite-difference time-domain (FDTD) model is employed to compute the electromagnetic fields in the simulation.**

I. Introduction

CURRENT density imaging (CDI) is an imaging technique that measures the electrical current density distribution based on magnetic resonance imaging (MRI). The non-invasiveness and the high spatial resolution inherited from MRI makes CDI an ideal measurement of current density and current flow inside biological objects[1]. Radio frequency current density imaging (RF-CDI) [2],[3]is a branch of CDI that measures electrical current density at the Larmor frequency. The Larmor frequencies of most MR imagers are in the radio frequency (RF) range, hence the name radio frequency current density imaging.

In CDI techniques, currents are applied to the object to be imaged externally by electrodes. RF-CDI is potentially applicable in biomedical applications, because radio frequency current does not stimulate nerves and muscles[4] . Recently implemented multi-slice RF-CDI technique has enhanced the potential of RF-CDI for biological and clinical applications by extending its ability to image multi-slice RF current density.

Manuscript received April 24, 2006. This work was supported in part by Natural Sciences and Engineering Research Council (NSERC) of Canada and in part by Communications and Information Technology Ontario (CITO) in Canada.

D. Wang is with the Institute of Biomaterials and Biomedical Engineering and with the Department of Electrical and Computer Engineering, University of Toronto, Toronto, ON M5S 3G9 Canada (phone: 416-946-7872; fax: 416-978-4317;e-mail: dinghui.wang@utoronto.ca).

T. P. DeMonte is with Field Metrica Inc., Toronto, ON M8V 1W1 Canada (e-mail: tdemonte@fieldmetrica.com).

M. L. Joy is with the Institute of Biomaterials and Biomedical Engineering and with the Department of Electrical and Computer Engineering, University of Toronto, Toronto, ON M5S 3G9 Canada (e-mail: mikejoy@ecf.utoronto.ca).

A. I. Nachman is with the Department of Mathematics and with the Department of Electrical and Computer Engineering, University of Toronto, Toronto, ON M5S 3G4 Canada (e-mail: adrian.nachman@utoronto.ca).

The thermal noise of MRI affects the precision and the interpretation of CDI measurement. It also defines a fundamental limit of the sensitivity of the measurement. In LF-CDI and single-slice RF-CDI, CDI measures phase information from complex MRI images to calculate current density distribution. Therefore, the standard deviation of the reconstructed current density noise is proportional to the reciprocal of the signal to noise ratio (SNR) of MRI and a general form of current density noise was derived [2]. However, unlike LF-CDI and single-slice RF-CDI, multi-slice RF-CDI does not encode the current density information in MRI phase images directly. Instead, each twist angle due to the magnetic component produced by RF current is calculated from four complex images by arc tangent operation [5]. Therefore, the general form of current density noise needs to be modified and parameters need to be clarified for multi-slice RF-CDI.

The goal of this paper is to analyze the current noise due to MRI random noise. First, a formula for the standard deviation of the current density noise is derived. Then, simulations that include a 3-D finite-difference time-domain (FDTD) model for the RF electromagnetic fields are utilized to verify the formula. Multi-slice RF-CDI experiment data are also analyzed.

II. Methodology

A. Theoretical Analysis

With the assumption that the current flows mainly in the direction of the static magnetic field $\mathbf{B_0}$, RF current density can be estimated by

$$J_z = 2\left(\frac{\partial \tilde{H}_y}{\partial x} - \frac{\partial \tilde{H}_x}{\partial y}\right) + 2j\left(\frac{\partial \tilde{H}_x}{\partial x} + \frac{\partial \tilde{H}_y}{\partial y}\right). \qquad (1)$$

In equation (1), J_z is the phasor form of total current density in the direction of main magnetic field $\mathbf{B_0}$ or the z direction by convention. $\tilde{H}_x$ and $\tilde{H}_y$ represent the transverse magnetic field components produced by the Larmor frequency current in the rotating frame [2].

The effects of $\tilde{H}_x$ and $\tilde{H}_y$ are to rotate the magnetization $\mathbf{M}$ away from the z axis and they are proportional to the twist angles Γ_x and Γ_y, respectively [3]. In the multi-slice RF-CDI sequence, components of $\mathbf{M}$ are stored in $\pm z$ axis and turned to the transverse plane and measured slice by slice. Four complex images, C^x_{y+}, C^x_{y-}, C^x_{z+} and C^x_{z-}, are acquired to estimate Γ_x and the other four are for Γ_y [5]. Γ_x is computed through arc tangent ($\tan^{-1}$) or arc cotangent

($\cot^{-1}$)operations.

$$\Gamma_x = \begin{cases} \tan^{-1}\left[\mathrm{Re}(C_y^x / C_z^x)\right] & if \left|C_z^x\right| \geq \left|C_y^x\right| \\ \cot^{-1}\left[\mathrm{Re}(C_z^x / C_y^x)\right] & if \left|C_z^x\right| < \left|C_y^x\right| \end{cases} \quad (2)$$

where

$$\begin{cases} C_y^x = C_{y+}^x - C_{y-}^x \\ C_z^x = C_{z+}^x - C_{z-}^x \end{cases}. \quad (3)$$

We write the complex images in real and imaginary form

$$C_{y+}^x = R_{y+}^x + iI_{y+}^x. \quad (4)$$

Now consider independent Gaussian random noise with mean zero and variance σ^2 added to the real and imaginary parts of the MR images. We denote the random noise δR_{y+}^x , δI_{y+}^x and likewise.

The measured twist angle $\Gamma_x + \delta\Gamma_x$ can then be expanded in a Taylor series around the true value Γ_x by considering Γ_x as a function of R_{y+}^x , I_{y+}^x , R_{y-}^x and so on. With high MR signal to noise ratio (SNR), truncating Taylor series up to the linear term is a good approximation for $\delta\Gamma_x$ [6]. Using this approach we obtain the mean and variance of $\delta\Gamma_x$. The mean value of $\delta\Gamma_x$ is

$$\overline{\delta\Gamma_x} = 0 \ . \quad (5)$$

Therefore, the variance of $\delta\Gamma_x$ is given by $\overline{\delta\Gamma_x^2}$

$$\overline{\delta\Gamma_x^2} = \frac{e^{2(t/T_1 + T_E/T_2^*)}}{2\left|\mathbf{M}\right|^2}\sigma^2, \quad (6)$$

in which t is time between event of the component of the magnetization stored in the z axis and the event of the component turned to the transverse plane for measurement. $\left|\mathbf{M}\right|$ is the magnitude of magnetization at time $t = 0$. T_1 and T_2^* are the longitudinal relaxation time constant and the effective transverse relaxation time constant, respectively. T_E is the echo time. If we define the reference image as the MR image with no current applied and the magnetization turned to the transverse plane at time 0, then $\left|\mathbf{M}\right|e^{-T_E/T_2^*}$ is the signal of the reference image magnitude. Therefore, the standard deviation of Γ_x is

$$\sigma_{\Gamma_x} = \frac{e^{t/T_1}}{\sqrt{2}SNR}. \quad (7)$$

SNR is the MRI signal to noise ratio of the reference image. Finally, the standard deviation of noise in either real part or imaginary part of current density is

$$\sigma_J = \frac{\sqrt{2}e^{t/T_1}}{\gamma\mu_0 T_c SNR}\sqrt{\left(\frac{F_x}{\Delta x}\right)^2 + \left(\frac{F_y}{\Delta y}\right)^2}. \quad (8)$$

where T_c is the duration of applied current, γ is the gyromagnetic ratio and μ_0 is the magnetic permeability of free space. F_x and F_y are the derivative noise template weighting factors, while Δx and Δy are the pixel dimensions. For the cases that Sobel templates are used in this study, $F_x = F_y = \sqrt{3}/4$ [2].

t in equation (8) is different for each slice. It increases as the slice number increases. Therefore, equation (8) predicts that the current noise grows exponentially depending on T_1 as the slice number increases.

B. Simulation and Experiment Verification

A cylindrical phantom used in RF-CDI experiments with diameter 38mm and height 110mm is shown in Fig. 1 (a). Copper plate electrodes are placed on both ends, which are connected to copper wires. The phantom was filled with doped saline, which was made up of 0.154 M (0.9 g /100 ml) NaCl, and 8 mM (0.2 g/100 ml) $CuSO_4$ of distilled water, with the longitudinal relaxation time constant T_1 around 160ms. For this doped saline, conductivity $\sigma \approx 1.5$ S/m and relative permittivity $\varepsilon_r \approx 80$.

The electromagnetic fields produced by RF current for the cylindrical phantom were simulated by 3-D FDTD[7]. The computational domain is sketched in Fig. 1(b). Mur's second order absorbing boundary conditions were implemented on the boundaries. The dimensions for the 3-D Yee's cell were $\Delta x = \Delta y = \Delta z = 2\,\mathrm{mm}$. $\Delta t = 3.47 \times 10^{-12}$ s for the simulation. The thin electrodes and wires were represented by setting all tangential components of electric field to zero. The longitudinal wire was 138 mm long and its distance to the center of the axis of the phantom was 80mm.

A current source was placed in one cell along the wire as indicated in Fig. 1(b). A sinusoidal current excitation at

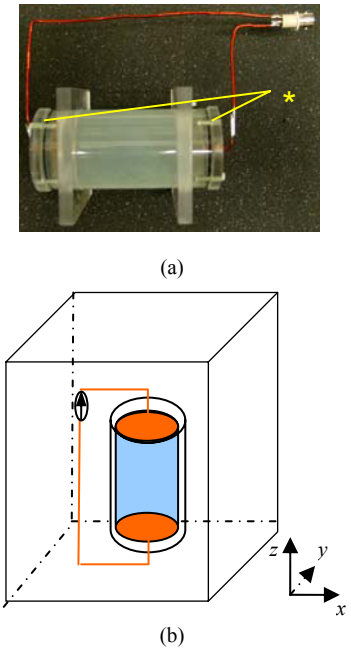

(a)

(b)

Fig 1 (a) A small cylindrical phantom used in RF-CDI experiments. * indicates the positions of electrodes. (b)Computational domain

frequency 64 MHz was implemented to approximate the applied current at the Larmor frequency for a 1.5 T MRI in time domain. When steady-state response was achieved, four points in one sinusoidal cycle were recorded at each cell, which were then converted to response in frequency domain by discrete Fourier transform.

The rotating frame components on seven transverse planes (xy planes) were calculated. With current duration $T_c = 8$ ms, the rotation angles were computed and converted to eight MR images for each slice. The magnitude of the reference MR image was normalized to unity and zero mean independent normally distributed noise with the standard deviation $1/SNR$ was added to both real and imaginary parts of each complex image. After current density was reconstructed according to (1), it was compared to the noiseless current density. With the differences of the two sets of images, current noise mean and standard deviation were evaluated.

Multi-slice RF-CDI experiments were performed using the phantom shown in Fig. 1(a) in a 1.5 T clinical MR imager without current applied. $T_c = 8$ ms for all the experiments. The mean and standard deviation of the current density were evaluated to investigate the random noise effects. The phantom was placed in the MR imager with its longitudinal axis aligned long the direction of $\mathbf{B_0}$.

III. Results

The simulation was calculated for around 20000 time steps. The current density along z direction was computed directly in FDTD simulation by generalized Ampere's law. The resulting waveform for a point at the center of the phantom in time domain is plotted in Fig. 2. After about one and a half cycles (about 23 ns), the waveform is almost in pure sinusoidal shape which indicates that the response to the excitation reaches the steady-state.

The steady-state electromagnetic field response in time domain was converted to phasor form. Fig. 3 shows the

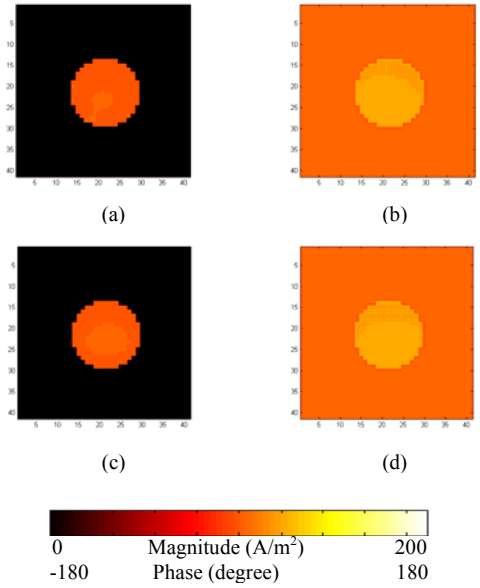

Fig. 3 Top: Jz magnitude (a) and phase(b) calculated)from rotating frame components.
Bottom: Jz calculated magnitude (c) and phase(d) directly

simulated current density magnitude and phase in z direction at one centre slice of the phantom. The magnitude and phase of current density computed by rotating frame components according to (1) are shown in Fig. 3 (a) and (b). They are very similar to the magnitude and phase of J_z simulated directly from the FDTD model which are shown in Fig. 3 (c) and (d).

Current density noises were evaluated in either real or imaginary parts of the reconstructed current density at different simulated current levels with different MRI SNR values. The results are consistent with that predicted by (8). When SNR of current density is high, the standard deviation of noise evaluated in current density magnitude is

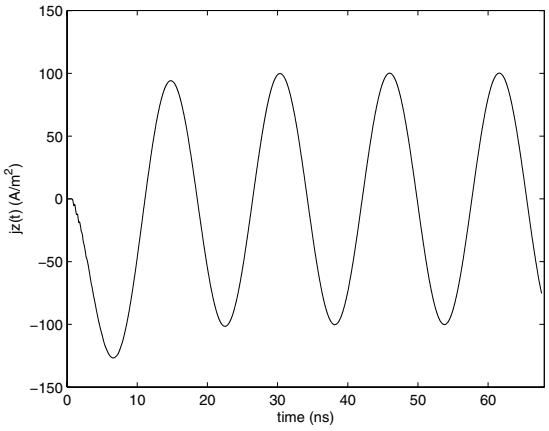

Fig. 2 Current density along the z direction at the center of the phantom

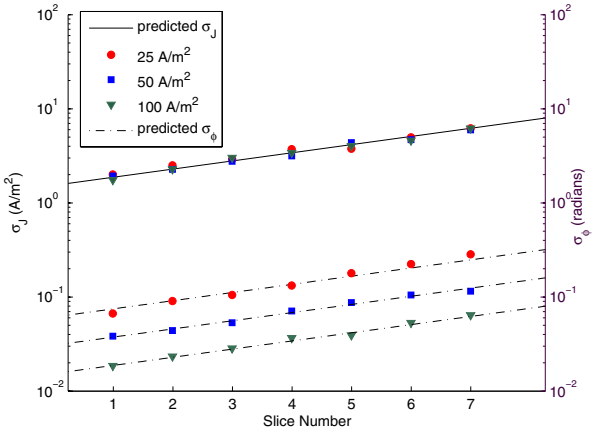

Fig. 4 Noise estimations for current density magnitude and phase at different current density level

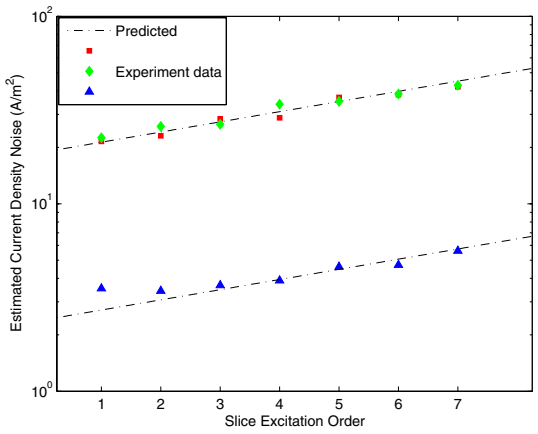

Fig. 5 Experimental current noise evaluation with zero current applied to the phantom

approximately the standard deviation of current density noise evaluated in real and imaginary parts of current density, and the standard deviation of current phase noise is close to the reciprocal of current density magnitude SNR in radians. Fig. 4 shows the estimated standard deviations of current density magnitude and phase noise at current density level 25, 50 and 100 A/m^2 for seven slices. $T_1 = 160$ ms in the simulations. MRI SNR is 100 for all these three cases. The horizontal axis indicates the slice number. The current density magnitude noise and phase noise are plotted in log scales. We can see that the current noise evaluated from the simulations matches the predicted magnitude noise (solid line) and phase noise (dash-dot line) very well. Current noise increases exponentially as the slice number increases.

Fig. 5 shows the results of estimated current density noise from seven slices for experiments without current applied. T_1 was about 160 ms for these experiments. Standard deviation was evaluated in real part of the reconstructed current density. Current density noise increases with respect to the slice order, and the increasing trend is close to the predicted exponential curves. Because of different imaging parameters, MRI SNR was around 112 for one experiment and 28 for the other two. Δx and Δy in the first one are double the sizes of the rest two. Therefore, as predicted, the current noise increases by a factor of 8 in the later case.

IV. Discussion

In multi-slice RF-CDI, the current density random noise increases exponentially with respect to T_1. Therefore, in biomedical applications, the relaxation rates of tissues to be imaged will constrain the number of slices that can be imaged. At a rough estimation, for most biological tissues that are commonly imaged by MRI, multi-slice RF-CDI will be able to image around 5 to 20 slices.

Random noise performance should also be analyzed at various current levels in RF-CDI experiments. Mean and standard deviation of current density were estimated for RF-CDI experiment with mean current density around 97 A/m^2[5]. The estimated standard deviations were much larger compared to the current noise predicted by (8). One possible reason is that the noiseless current density distribution might not be perfectly uniform in each slice. In fact, in the FDTD simulation results (Fig. 3), minor variations due to the relative positions with regard to the return wires in both magnitude and phase images of J_z are observed. An appropriate way to estimate the random noise performance in experiments is to compare the reconstructed current density with the one from numerical calculation. This will require careful registration of phantom and return wires between the FDTD simulation and the experiment. A more practical alternative is to evaluate the standard deviations of current density noise pixel by pixel from a set of RF-CDI experiments with the same amount of current applied[8].

V. Conclusion

In this paper, random noise performance for multi-slice RF-CDI has been analyzed theoretically and verified by simulations and experiments The results have shown that the sensitivity to random noise of each slice is dependent on the longitudinal relaxation time constant T_1.

Acknowledgment

D. Wang would like to thank Dr. Cotas D. Sarris in University of Toronto for providing the original Matlab code for 3-D FDTD simulation.

References

[1] R. S. Yoon, T. P. DeMonte, K. F. Hasanov, D. B. Jorgenson, and M. L. G. Joy, "Measurement of thoracic current flow in pigs for the study of defibrillation and cardioversion," *IEEE Trans. Biomed. Eng.*, vol. 50, no. 10, pp. 1167-1173, 2003.

[2] G. C. Scott, "NMR imaging of current density and magnetic fields." Ph.D. Elec. Eng., Univ. Toronto, ON, Canada, 1993.

[3] G. C. Scott, M. L. G. Joy, R. L. Armstrong, and R. M. Henkelman, "Rotating-frame RF current density imaging," *Magn. Reson. Med.*, vol. 33, no. 3, pp. 355-369, 1995.

[4] J. C. Griffin, "Physiological effects of electric currents on living organisms, more particularly humans," in *Electrical shock safety criteria: proceedings of the first international symposium on electrical shock safety criteria*, J. Bridges, Ed. 1983, pp. 7-24.

[5] D. Wang, "Multi-slice radio frequency current density imaging." Elec. Eng., Univ. Toronto, ON, Canada, 2004.

[6] E. M. Haacke, R. W. Brown, M. R. Thompson, and R. Venkatesan, "Signal, contrast and noise," in *Magnetic resonance imaging physical principles and sequence design*, John Wiley & Sons, Inc., 1999, pp. 331-380.

[7] A. Taflove and S. Hagness, *Computational electrodynamics:the finite difference time domain method* Artech House, 2000.

[8] R.S. Yoon, "Biological applications of current density imaging." Ph.D. Elec. Eng., Univ. Toronto, ON, Canada, 2003.